

Dirac electrons in the square-lattice Hubbard model with a d -wave pairing field: The chiral Heisenberg universality class revisited

Yuichi Otsuka,^{1,*} Kazuhiro Seki,² Sandro Sorella,^{1,3,4} and Seiji Yunoki^{1,2,5}

¹*Computational Materials Science Research Team,*

RIKEN Center for Computational Science (R-CCS), Kobe, Hyogo 650-0047, Japan

²*Computational Quantum Matter Research Team,*

RIKEN Center for Emergent Matter Science (CEMS), Wako, Saitama 351-0198, Japan

³*SISSA – International School for Advanced Studies, Via Bonomea 265, 34136 Trieste, Italy*

⁴*Democritos Simulation Center CNR–IOM Istituto Officina dei Materiali, Via Bonomea 265, 34136 Trieste, Italy*

⁵*Computational Condensed Matter Physics Laboratory, RIKEN, Wako, Saitama 351-0198, Japan*

(Dated: February 14, 2022)

We numerically investigate the quantum criticality of the chiral Heisenberg universality class with the total number of fermion components $N = 8$ in terms of the Gross-Neveu theory. Auxiliary-field quantum Monte Carlo simulations are performed for the square lattice Hubbard model in the presence of a d -wave pairing field, inducing Dirac cones in the single-particle spectrum. This property makes the model particularly interesting because it turns out to belong to the same universality class of the Hubbard model on the honeycomb lattice, which is the canonical model for graphene, despite the unit cells being apparently different (e.g., they contain one and two sites, respectively). We indeed show that the two phase transitions, expected to occur on the square and on the honeycomb lattices, have the same quantum criticality. We also argue that details of the models, i.e., the way of counting N and the anisotropy of the Dirac cones, do not change the critical exponents. The present estimates of the exponents for the $N = 8$ chiral Heisenberg universality class are $\nu = 1.05(5)$, $\eta_\phi = 0.75(4)$, and $\eta_\psi = 0.23(4)$, which are compared with the previous numerical estimations.

I. INTRODUCTION

The study of quantum critical points in Dirac fermions has received increased attention across many research fields. Massless Dirac fermions emerge as quasiparticles in various condensed-matter systems [1, 2]. The Coulomb interaction among electrons is almost inevitable even within the quasiparticle picture, and so far the most popular models adopted to describe the electron correlation in the Dirac fermions are standard Hubbard models of which the kinetic-energy parts are characterized by linear dispersions near the Fermi level. Numerical studies on these models have typically found evidence of a Mott transition between a semimetal (SM) and an anti-ferromagnetic (AF) insulator [3–11]. Further analytical studies motivated by graphene [12–15] have revealed that an effective theory for the Mott transition is described by the Gross-Neveu (GN) model [16], a well-studied effective model in high-energy physics [17–23]. Since it had been predicted by the GN theory that the phase transitions of the interacting Dirac fermions are classified into three universality classes, namely chiral Ising, chiral XY, and chiral Heisenberg classes, corresponding to the Z_2 , $U(1)$, and $SU(2)$ symmetry breaking, a number of quantum Monte Carlo (QMC) calculations have been performed on various lattice models realizing quantum phase transitions in the Dirac fermions [24–43]. The proliferation of numerical studies on these lattice models has also led to a renewed interest in the continuum GN model [44–49].

Since a universality class is characterized and distinguished by a set of critical exponents, the evaluation of the critical exponents is of general interest, and particularly challenging for theorists. In spite of considerable efforts devoted to determine the critical exponents of the GN universality classes, only partial agreement between different theoretical methods has been achieved; in particular large discrepancies between numerical and analytical approaches have remained. Indeed, a satisfactory consistency has been found only for the $N = 4$ chiral Ising class (N denotes the total number of fermion components) [31, 49], and other classes including the $N = 8$ chiral Heisenberg class, which is of particular interest because of its tight connection with graphene [12–15], have to be further explored.

It should also be pointed out that the critical exponents are not only a subject of purely academic interest but are also practically useful to identify the phase transitions. Such examples are found in the studies of the honeycomb bilayer model [50], the Kekulé valence-bond-solid transition [29, 32], and the quantum spin Hall insulator transition [41].

In this paper, we investigate the quantum phase transition in another celebrated manifestation of Dirac fermions in condensed-matter physics: the spectrum of a d -wave superconductor (SC) [51, 52], showing clear nodal quasiparticles in the single-particle spectrum. Specifically, we consider an effective square lattice model of a d -wave SC in the presence of the Hubbard U interaction. In this model there are four Dirac cones for each spin component, and therefore the phase transition triggered by U should in principle belong to the $N = 8$ chiral Heisenberg class, the same universality class of the Hubbard model

* otsukay@riken.jp

on the honeycomb lattice (hereinafter referred to as the honeycomb lattice model) [3, 5–8, 10, 11, 36–39, 42], which is closely related to graphene [12–14, 53]. Thus the same critical exponents are expected as those for the honeycomb lattice model.

This is remarkable because the Hubbard model with the d -wave pairing field studied here, is apparently different from the honeycomb lattice model. First, the former model has four independent Dirac cones without sublattice in contrast to two Dirac cones with two sublattices for the latter model, while the total number of the fermion components is the same, i.e., $N = 8$ for both models. Second, in the d -wave SC, the Dirac cone is in general anisotropic, because the velocity at the Dirac point depends on the chosen direction in momentum space. From the point of view of renormalization group, the relativistic invariance may emerge at the critical point. However, the effect of the anisotropy on the quantum criticality cannot be studied in the honeycomb lattice model which has the isotropic Dirac cones. According to the notion of the universality class stating that the criticality does not depend on the details of the models, the critical exponents for both models should in principle be the same. Therefore we expect that our work represents a nontrivial test of this universality assumption for the exponents.

The rest of the paper is organized as follows. In the next section, the model is defined and the QMC method is briefly explained. In Sec. III, the results of the QMC simulations are analyzed by various methods such as a crossing-point analysis based on the phenomenological renormalization argument and a data-collapse method of the finite-size scaling ansatz. The obtained critical exponents are discussed in comparison with the previous estimations, before concluding the paper, in Sec. IV.

II. MODEL AND METHOD

A. Model

We study the two-dimensional Hubbard model at half filling with the d -wave BCS SC order parameter described by the following Hamiltonian:

$$H = H_{\text{BCS}} + H_U, \quad (1)$$

where

$$H_{\text{BCS}} = \sum_{\langle i,j \rangle} \left\{ \begin{pmatrix} c_{i\uparrow}^\dagger & c_{i\downarrow} \end{pmatrix} \begin{pmatrix} -t & \Delta_{ij} \\ \Delta_{ij}^* & t \end{pmatrix} \begin{pmatrix} c_{j\uparrow} \\ c_{j\downarrow} \end{pmatrix} + \text{h.c.} \right\} \quad (2)$$

and

$$H_U = U \sum_i n_{i\uparrow} n_{i\downarrow}. \quad (3)$$

Here, $c_{i\sigma}^\dagger$ creates an electron with spin σ ($=\uparrow, \downarrow$) at site i of position \mathbf{r}_i and $n_{i\sigma} = c_{i\sigma}^\dagger c_{i\sigma}$ is a number operator. In

the noninteracting part, H_{BCS} , t represents the transfer integral chosen as an energy unit, i.e., $t = 1$, and Δ_{ij} is the BCS SC order parameter, with the sum indicated by $\langle i, j \rangle$ running over all pairs of nearest-neighbor sites i and j . We consider the model on a square lattice of linear dimension L . The BCS order parameter Δ_{ij} with the d -wave symmetry is set to have a uniform amplitude Δ between the nearest-neighbor sites: $\Delta_{ij} = \Delta$ ($-\Delta$) for sites i and j aligned along the x (y) direction. In the interacting part of Eq. (3), U (> 0) denotes the repulsive interaction, which triggers the quantum phase transition from the SM [54] to the AF insulator, breaking both the chiral and SU(2) symmetries. Since we take into account the amplitude Δ as a model parameter, the U(1) symmetry is explicitly broken from the outset, and thus the AF insulator with two Goldstone modes [55, 56] coexists with the d -wave SC order. Note that, according to a very recent report [43], the U(1) symmetry plays no important role in the AF transition.

The noninteracting Hamiltonian of Eq. (2) is expressed in momentum space as follows:

$$H_{\text{BCS}} = \sum_{\mathbf{k}} \begin{pmatrix} c_{\mathbf{k}\uparrow}^\dagger & c_{-\mathbf{k}\downarrow} \end{pmatrix} \begin{pmatrix} \epsilon_{\mathbf{k}} & \Delta_{\mathbf{k}} \\ \Delta_{\mathbf{k}}^* & -\epsilon_{\mathbf{k}} \end{pmatrix} \begin{pmatrix} c_{\mathbf{k}\uparrow} \\ c_{-\mathbf{k}\downarrow}^\dagger \end{pmatrix}, \quad (4)$$

where

$$\epsilon_{\mathbf{k}} = -2t (\cos k_x + \cos k_y) \quad (5)$$

and

$$\Delta_{\mathbf{k}} = 2\Delta (\cos k_x - \cos k_y). \quad (6)$$

The energy dispersion of Bogoliubov quasiparticles is then obtained as $E(\mathbf{k}) = \pm (\epsilon_{\mathbf{k}}^2 + |\Delta_{\mathbf{k}}|^2)^{1/2}$, which has four independent Dirac points at $\mathbf{k} = (\pm\pi/2, \pm\pi/2)$ and $(\pm\pi/2, \mp\pi/2)$ as shown in Fig. 1. Together with the spin degrees of freedom, the effective model in the continuum limit is the GN model with a total number of fermion components $N = 8$ [57–59], which is the same as the honeycomb lattice model or the Hubbard model on the square lattice with π flux (referred to as the π -flux model in the following) [4, 9, 10, 37, 38], although the counting of the fermion components is different: two Dirac cones, two sublattices, and two spin components in the latter models.

The Dirac cones described by H_{BCS} are in general anisotropic, i.e., elliptic cones, and the ellipticity is determined by $|\Delta/t|$. To be concrete, let us focus on the low-lying excitations around one Dirac point at $\mathbf{k}_D = (\pi/2, \pi/2)$. The energy dispersion can be expanded with a small wave vector $\delta\mathbf{k} = \mathbf{k} - \mathbf{k}_D = (\delta k_x, \delta k_y)$ as $E(\mathbf{k}_D + \delta\mathbf{k}) \approx \pm \mathcal{E}(\delta\mathbf{k})$, where

$$\mathcal{E}(\delta\mathbf{k}) = \sqrt{v_F^2 \left(\frac{\delta k_x + \delta k_y}{\sqrt{2}} \right)^2 + v_\Delta^2 \left(\frac{\delta k_x - \delta k_y}{\sqrt{2}} \right)^2} \quad (7)$$

and the nodal Fermi velocity $v_F \equiv 2\sqrt{2}t$ (the gap velocity $v_\Delta \equiv 2\sqrt{2}|\Delta|$) is the velocity perpendicular (parallel) to the Fermi surface of H_{BCS} with $\Delta = 0$ at half

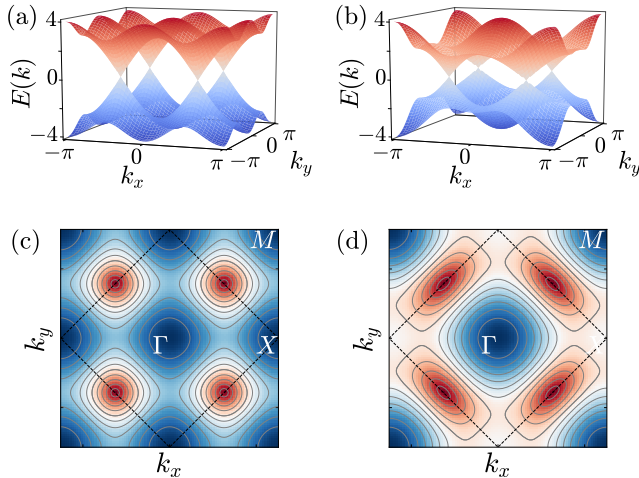


FIG. 1. The noninteracting energy dispersion $E(\mathbf{k})$ for (a) $\Delta = 1$ and (b) $\Delta = 0.5$, and the corresponding contour plot of the lower band for (c) $\Delta = 1$ and (d) $\Delta = 0.5$. In panels (c) and (d), high symmetric momenta are denoted Γ for $\mathbf{k} = (0, 0)$, X for $\mathbf{k} = (\pi, 0)$, and M for $\mathbf{k} = (\pi, \pi)$, and the Fermi surface in the case of $\Delta = 0$ is indicated by dashed lines.

filling. The Dirac cone becomes isotropic if and only if $|\Delta/t| = 1$, as shown in Fig. 1(c), and otherwise it is elliptic, as shown in Fig. 1(d) [60]. Therefore, our model is considered as a tunable model, where the velocity is controllable and the Dirac cone can be deformed elliptically with the Dirac points kept at $\mathbf{k} = (\pm\pi/2, \pm\pi/2)$ and $(\pm\pi/2, \mp\pi/2)$. This is a convenient feature, allowing us to study the putative universal nature of the phase transitions based on lattice model simulations.

The quasiparticle density of states $D(E)$ per site close to the Dirac point is given as

$$D(E) = \frac{2\pi N_{\text{Dirac}}}{\bar{v}^2 V_{\text{BZ}}} |E|, \quad (8)$$

where N_{Dirac} is the number of Dirac points in the Brillouin zone (BZ), V_{BZ} is the volume of the BZ, and \bar{v} is the geometric mean of v_F and v_Δ , i.e., $\bar{v} = \sqrt{v_F v_\Delta}$. Note that Eq. (8) also holds for the honeycomb lattice model and the π -flux model. Therefore, \bar{v} plays essentially the same role as the Dirac Fermi velocity v_F^0 in the isotropic model.

B. Method

The model described by the Hamiltonian H in Eq. (1) is investigated by the auxiliary-field quantum Monte Carlo (AFQMC) method [61–65] at half filling, where the fermionic negative-sign problem does not occur. An expectation value of a physical observable O at zero temperature is calculated for the ground-state wave function projected from a left (right) trial wave function $\langle\psi_L|$

$(|\psi_R\rangle)$,

$$\langle O \rangle = \frac{\langle\psi_L|e^{-\frac{\beta}{2}H} O e^{-\frac{\beta}{2}H}|\psi_R\rangle}{\langle\psi_L|e^{-\beta H}|\psi_R\rangle}, \quad (9)$$

where projection time denoted by β is set to be proportional to L with the Lorentz invariance assumed [13, 14]. A slice of the Suzuki-Trotter decomposition [66, 67] is chosen as $\Delta\tau = \beta/M = 0.1$ with M being integer, which is confirmed to result only in negligible systematic errors compared with statistical errors in the Monte Carlo sampling. The discrete Hubbard-Stratonovich transformation [68] is employed to decouple the interaction term $e^{-\Delta\tau H_U}$, which introduces a real auxiliary Ising field coupled to spin at each site in space and imaginary time. The simulations are performed on finite-size lattices of $L = 8, 12, 16, 20, 24, 32, 40$ with periodic boundary conditions for several values of U below and above the quantum critical point U_c of the phase transition.

III. RESULTS

A. crossing-point analysis

Using AFQMC, we calculate the spin structure factor defined as

$$S(\mathbf{k}) = \frac{1}{L^2} \sum_{i,j} e^{i\mathbf{k}(\mathbf{r}_i - \mathbf{r}_j)} \langle \mathbf{S}_i \cdot \mathbf{S}_j \rangle, \quad (10)$$

where $\mathbf{S}_i = \frac{1}{2} \sum_{s,s'} c_{is}^\dagger (\boldsymbol{\sigma})_{ss'} c_{is'}$ is the spin operator with $\boldsymbol{\sigma} = (\sigma_x, \sigma_y, \sigma_z)$ being the vector of Pauli matrices. For large U , $S(\mathbf{k})$ is peaked at the AF ordering momentum, $\mathbf{K} = (\pi, \pi)$. The critical point U_c of the AF transition can be located by monitoring the correlation ratio,

$$R_{m^2}(U, L) = 1 - \frac{S(\mathbf{K} + \mathbf{b}/L)}{S(\mathbf{K})}, \quad (11)$$

where \mathbf{b} denotes the smallest reciprocal-lattice vector. In the AF ordered phase, $R_{m^2}(U, L)$ scales to 1 in the thermodynamic limit, as the Bragg peak in $S(\mathbf{k})$ becomes infinitely sharp. On the other hand, $R_{m^2}(U, L)$ decreases to 0 as $L \rightarrow \infty$ in the disordered phase. At the critical point, the correlation ratio becomes volume independent; it is expected to cross at a universal value for different L , by which feature we can determine the critical point in a sensitive way [50, 69]. However, if there are non-negligible corrections to the scaling, the crossing points of $R_{m^2}(U, L)$ drift with increasing L . We clearly observe this drift as shown in Fig. 2, which is in contrast with the recent study of SLAC fermions [40]. In the presence of the corrections, the crossing-point analysis [70] serves as a simple and reliable way to find the critical point, which has been developed mainly in quantum spin systems [70–75] and has also recently been applied to fermionic models [27, 29, 30, 35, 37, 41, 76].

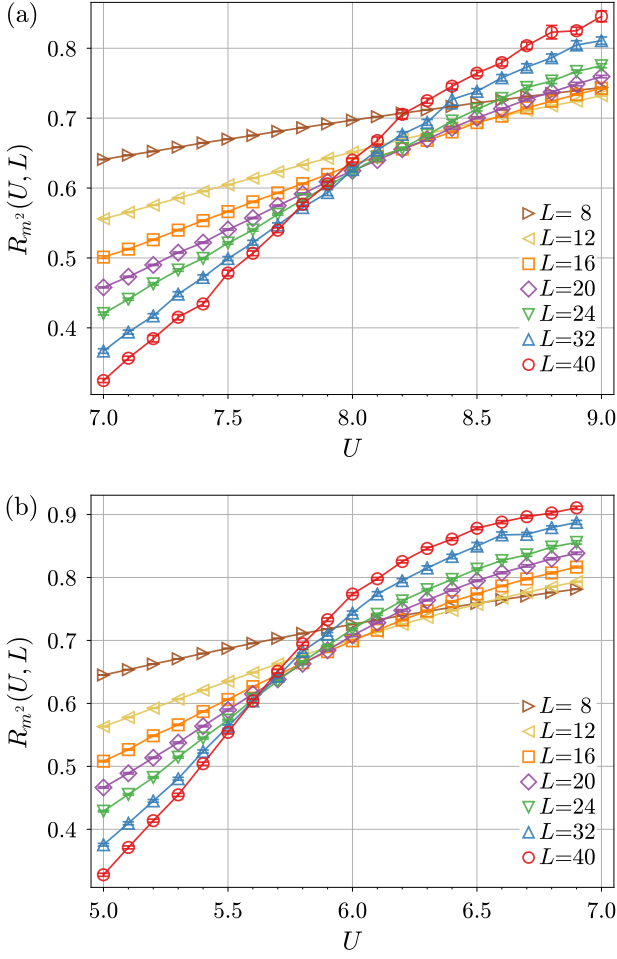


FIG. 2. Correlation ratio $R_{m^2}(U, L)$ of spin structure factor as a function of U for various system sizes L ; (a) $\Delta = 1$ and (b) $\Delta = 0.5$.

A crossing point denoted by $U^\times(L, rL)$ is defined as a value of U at which two curves of $R_{m^2}(U, L)$ and $R_{m^2}(U, rL)$ cross, which we compute by polynomial interpolation. Based on the phenomenological renormalization argument, the crossing points are extrapolated to the critical point following a simple power law [70]:

$$U^\times(L, rL) = U_c + cL^{-(\omega+1/\nu)}, \quad (12)$$

where c is a constant, ω is an exponent of the leading correction term, and ν is the correlation-length exponent. We choose the ratios of the two system sizes as $r = 2$ and $r = (L+8)/L$, each of which covers all the lattice sizes L ($= 8, 12, 16, 20, 24, 32, 40$). The results show that both series for each Δ are extrapolated to the same U_c within the error bars; $U_c = 7.63(4)$ and $7.61(5)$ for $\Delta = 1$ [Fig. 3(a)], and $U_c = 5.49(3)$ and $5.47(3)$ for $\Delta = 0.5$ [Fig. 3(b)]. The fitted exponents in Eq. (12), i.e., $\omega + 1/\nu$ fall in almost the same value for each r irrespectively of Δ ; $\omega + 1/\nu = 1.8(1)$ for $r = 2$, and $\omega + 1/\nu = 1.4(1)$ for $r = (L+8)/L$. If the phase transitions for $\Delta = 1$

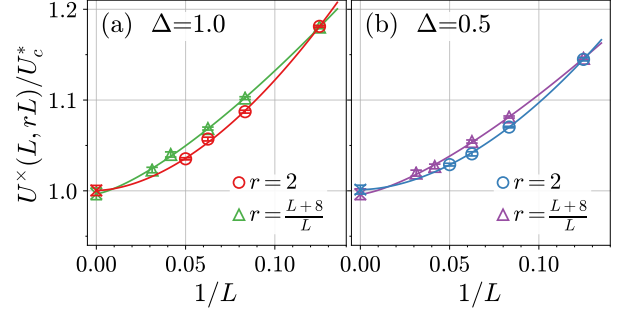


FIG. 3. Crossing-point analysis of the correlation ratio. $U^\times(L, rL)$ are obtained by interpolating data points of $R_{m^2}(U, L)$ with second-order polynomial functions. For ease of comparison, values of $U^\times(L, rL)$ are normalized by $U_c^* = 7.63$ and 5.49 for (a) $\Delta = 1$ and (b) $\Delta = 0.5$, respectively. Ratios of two system sizes are $r = 2$ (circles) and $r = (L+8)/L$ (triangles). Results of the fit with $U^\times(L, rL) = U_c + dL^{-(\omega+1/\nu)}$ are (a) $U_c = 7.63(4)$ and $\omega + 1/\nu = 1.8(1)$ for $r = 2$ and $U_c = 7.61(5)$ and $\omega + 1/\nu = 1.4(1)$ for $r = (L+8)/L$, and (b) $U_c = 5.49(3)$ and $\omega + 1/\nu = 1.8(1)$ for $r = 2$ and $U_c = 5.47(3)$ and $\omega + 1/\nu = 1.4(1)$ for $r = (L+8)/L$. Numbers in parentheses denote errors in the last digits. Note that U_c s extrapolated in the thermodynamic limit are indicated by crosses at $1/L = 0$.

and 0.5 belong to the same universality class, both ν and ω should be universal, resulting in the same value of $\omega + 1/\nu$. This is indeed the case in our result for each r . The difference in $\omega + 1/\nu$ between $r = 2$ and $(L+8)/L$ is speculated to be due to large corrections to the scaling. Even with the large corrections, Eq. (12) can be exploited by considering the exponent ω as an effective one which implicitly includes effects of higher-order corrections [70, 75]. Our result may imply that ν is universal with the effective ω which is dependent on the fitting condition, such as the choice of r .

The correlation-length exponent ν itself can be estimated by the crossing-point analysis [70]. Since we have used the polynomial interpolation of $R_{m^2}(U, L)$ to find $U^\times(L, rL)$, it is straightforward to compute its slope, $s(U, L) = \frac{dR_{m^2}(U, L)}{dU}$. The size-dependent inverse correlation-length exponent is calculated from ratio of the two slopes at the crossing point,

$$\frac{1}{\nu(L, rL)} = \frac{1}{\ln(r)} \ln \left\{ \frac{s(U^\times, rL)}{s(U^\times, L)} \right\}, \quad (13)$$

where U^\times stands for a shortened form of $U^\times(L, rL)$. This quantity scales to the correct exponent at the rate $L^{-\omega}$,

$$\frac{1}{\nu(L, rL)} = \frac{1}{\nu} + dL^{-\omega}, \quad (14)$$

where d is a constant and ω is the correction exponent. Since the evaluation of the slope is rather sensitive and affected by the small number of the data points of $R_{m^2}(U, L)$, the fit to the data turns out to be difficult.

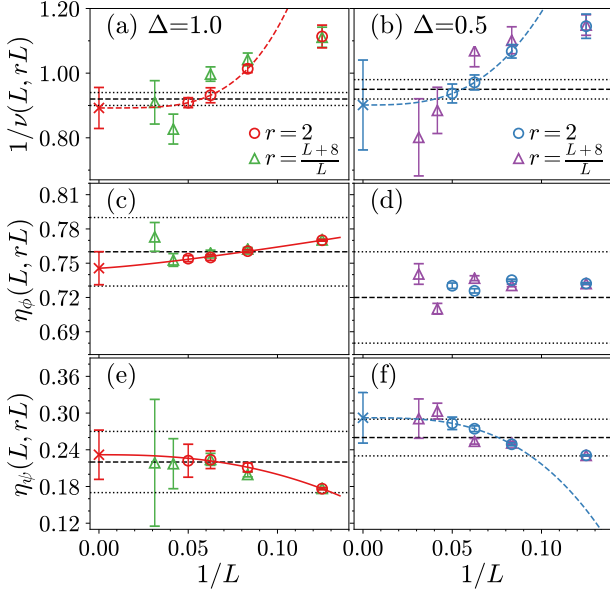


FIG. 4. System size dependence of (a), (b) the inverse correlation-length exponent $1/\nu$, (c), (d) the anomalous dimension for the order parameter η_ϕ , and (e), (f) the anomalous dimension for the fermionic field η_ψ . Left (right) panels show results for $\Delta = 1$ (0.5). Ratios of two system sizes are $r = 2$ (circles) and $r = (L + 8)/L$ (triangles). Solid and dashed lines are fits to data of $r = 2$ with and without $L = 8$, respectively, from which the exponents are estimated as (a) $\nu = 1.12(8)$, (b) $\nu = 1.11(17)$, (c) $\eta_\phi = 0.75(2)$, (e) $\eta_\psi = 0.23(4)$, and (f) $\eta_\psi = 0.29(4)$, indicated by crosses at $1/L = 0$. Here, numbers in parentheses denote errors in the last digits. In the other cases, fitted lines are not shown, because the fits are unstable. Horizontal dashed and dotted lines represent values of the exponents and their error bars estimated from slopes of log-log plots of $m^2(U_c, L)$, $Z(U_c, L)$, and $s(U_c, L)$ in Figs. 5, 6, and 7.

Nonetheless, the fit without $L = 8$ for $r = 2$ yields consistent values of $\nu = 1.12(8)$ and $1.11(17)$ for $\Delta = 1$ and 0.5 , respectively, as shown in Figs. 4(a) and 4(b). The correction exponent ω is expected to be the same as that in Eq. (12), especially since basically the same quantity, $R_{m^2}(U, L)$, is examined here. However, the resultant ω in Figs. 4(a) and 4(b) are larger than those expected from $\omega + 1/\nu = 1.4 - 1.8$ in Fig. 3 and $\nu \simeq 1.1$. The analysis based on Eq. (12) is more straightforward, and thereby we expect that it is more reliable than the analysis based on Eq. (13). The exponent ω in the latter case should be considered as an independent fitting parameter to estimate ν .

B. scaling at the critical point

In the GN scenario, the phase transition, namely spontaneous symmetry breaking, accompanies with opening a charge gap [15, 16]. Thus, it is characterized by two

quantities, the staggered magnetization $m^2(U, L)$ and the quasiparticle weight $Z(U, L)$. In the QMC simulations, $m^2(U, L)$ is calculated from the spin structure factor in Eq. (10) as

$$m^2(U, L) = S(\mathbf{K})/L^2. \quad (15)$$

$Z(U, L)$ is also estimated as follows [33, 77]:

$$Z(U, L) = \frac{D_\sigma(U, L)}{D_\sigma(0, L)}, \quad (16)$$

where $D_\sigma(U, L) = \frac{1}{L^2} \sum_i \langle c_{j\sigma}^\dagger c_{i\sigma} \rangle$ is the equal-time single-particle Green's function at the maximum distance, $\mathbf{r}_j - \mathbf{r}_i = (L/2, L/2)$. At the critical point, these two quantities scale as

$$m^2(U_c, L) \propto L^{-1-\eta_\phi} (1 + gL^{-\omega}), \quad (17)$$

and

$$Z(U_c, L) \propto L^{-\eta_\psi} (1 + hL^{-\omega}), \quad (18)$$

where η_ϕ (η_ψ) is the anomalous dimension for the order parameter (fermionic field), and the effective correction terms to the first order are taken into account with g and h being constants. The exponents ω are taken into account as independent fitting parameters. Similar to Eq. (13), the size-dependent exponents can be defined by taking the two system sizes L and rL as

$$\eta_\phi(L, rL) = \frac{1}{\ln(r)} \ln \left\{ \frac{m^2(U_c, L)}{m^2(U_c, rL)} \right\} - 1 \quad (19)$$

and

$$\eta_\psi(L, rL) = \frac{1}{\ln(r)} \ln \left\{ \frac{Z(U_c, L)}{Z(U_c, rL)} \right\}. \quad (20)$$

From these quantities, the exponents are extrapolated as

$$\eta_\phi(L, rL) = \eta_\phi + g'L^{-\omega} \quad (21)$$

and

$$\eta_\psi(L, rL) = \eta_\psi + h'L^{-\omega}, \quad (22)$$

where g' and h' are constants. The fits of the data according to these forms are again rather difficult, as shown in Figs. 4(c)-4(f), some of which however yield the estimations as $\eta_\phi = 0.75(2)$ for $\Delta = 1$ and $r = 2$, $\eta_\psi = 0.23(4)$ for $\Delta = 1$ and $r = 2$, and $\eta_\psi = 0.29(4)$ for $\Delta = 0.5$ and $r = 2$. Although the estimate of η_ϕ for $\Delta = 0.5$ is not available because of limitation in the quality of data, it seems consistent with that for $\Delta = 1$.

We also estimate the exponents η_ϕ and η_ψ by a more naive method without assuming a specific form of the correction term. Although $m^2(U, L)$ is expected to decay as $L^{-1-\eta_\phi}$ only at $U = U_c$ and for large L , here we try to fit the data points of $m^2(U, L)$ to a function

AL^{-1-a} with two, A and a , fitting parameters, regardless of whether U is close to U_c . At each U , the range of the fit is chosen as $L \in [L_{\min}, L_{\max}(=40)]$ and we examine how the fitted exponent a changes with increasing L_{\min} . Since $m^2(U=0, L)$ decays as L^{-2} , a is expected to approach 1 for $U < U_c$, whereas it should converge to η_ϕ at $U = U_c$. As shown in Figs. 5(a) and 6(a), the asymptotic behavior of a indeed changes at $U \simeq U_c^*$ that is estimated from the crossing-point analysis in Fig. 3. At these critical points, we estimate η_ϕ from the slope of the log-log plots of $m^2(U = U_c^*, L)$ for $L \geq L_{\min} = 20$ [see insets of Figs. 5(a) and 6(a)] as $\eta_\phi = 0.76(3)$ and $0.72(4)$ for $\Delta = 1$ and 0.5 , respectively. These values are consistent with the estimations from Eqs. (21) and (22) [also see Figs. 4(c) and 4(d)] and imply that this exponent is the same, independently of Δ .

We apply the same analysis to the quasiparticle weight; $Z(U, L)$ is fit to the function BL^{-b} . Note that, in this case, since for $U < U_c$ the equal-time single-particle Green's function $D_\sigma(U, L)$ in Eq. (16) decreases as r^{-2} with r being the distance and for $U > U_c$ it decays exponentially [77], the fitted exponent b shows an abrupt change at $U \simeq U_c^*$, as shown in Figs. 5(b) and 6(b). This is naturally expected from the GN scenario that describes SM and a gapped ordered phase separated by a single phase transition, and at the same time provides further evidence for the accuracy of estimates of the critical point. The critical exponents estimated from the log-log plots at $U = U_c^*$, as shown in the insets of Figs. 5(b) and 6(b), again fall into the same value within the error bars; $\eta_\psi = 0.23(5)$ and $0.26(3)$ for $\Delta = 1$ and 0.5 , respectively.

Since it turns out that our U_c^* is a good estimation of U_c and the conventional log-log fits given above work well, we may as well evaluate $1/\nu$ from the log-log fit of $s(U, L)$, which is expected to behave at the critical point for large L as follows [72]:

$$s(U_c, L) \sim L^{1/\nu}. \quad (23)$$

From the fit in Fig. 7, the exponent is obtained as $\nu = 1.09(2)$ and $1.04(3)$ for $\Delta = 1$ and 0.5 , respectively, being consistent with the crossing-point analysis of $\nu(L, rL)$ shown in Figs. 4(a) and 4(b).

C. data collapse

Finally, the critical points and exponents are also assessed by collapsing data on the basis of the finite-size scaling ansatz,

$$R_{m^2}(U, L) = f_R(uL^{1/\nu}), \quad (24)$$

$$m^2(U, L) = L^{-1-\eta_\phi} f_m(uL^{1/\nu}), \quad (25)$$

and

$$Z(U, L) = L^{-\eta_\psi} f_Z(uL^{1/\nu}), \quad (26)$$

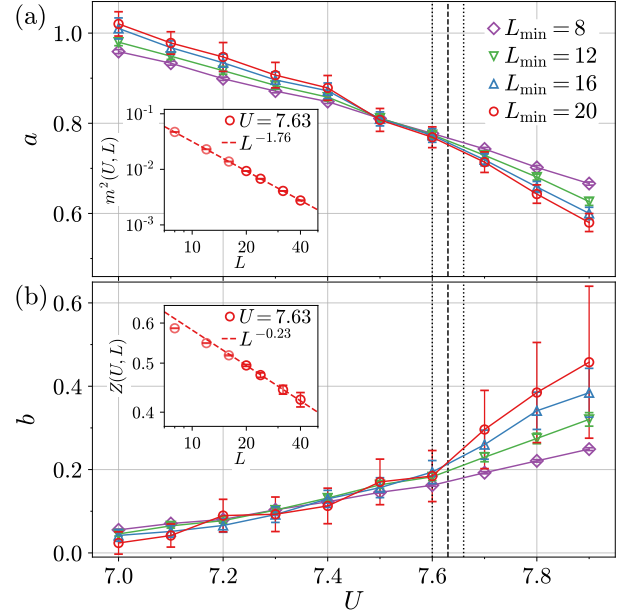


FIG. 5. U dependence of fitted exponents for $\Delta = 1$; (a) staggered magnetization $m^2(U, L)$ is fit to AL^{-1-a} and (b) quasiparticle weight $Z(U, L)$ is fit to BL^{-b} . Fitting range is between L_{\min} and $L_{\max}(=40)$. Vertical dashed and dotted lines indicate the critical point and the error bar, $U_c^* = 7.63(4)$, estimated from the crossing-point analysis of the correlation ratio in Fig. 3(a). Insets of panels (a) and (b) are log-log plots of $m^2(U_c^*, L)$ with $\eta_\phi = 0.76(3)$ and $Z(U_c^*, L)$ with $\eta_\psi = 0.22(5)$, respectively. Here, numbers in parentheses denote errors in the last digits.

where $u = (U - U_c)/U_c$ represents normalized distance from the critical point and f_α ($\alpha = R, m, Z$) the scaling functions. The correction terms are not explicitly included in the scaling form. Instead, as described in the second half of Sec. III B, we perform data collapsing for L between L_{\min} and L_{\max} and analyze trends of fit results with increasing L_{\min} [33, 38].

We employ the Bayesian method to tightly collapse the data without relying on using a specific polynomial function [78]. Figure 8 shows typical examples of the data collapses for $L_{\min} = 16$. From each of the collapse fits, the sets of U_c and ν are independently estimated. In addition, η_ϕ and η_ψ are also determined from the data collapse fits of $m^2(U, L)$ and $Z(U, L)$, respectively. Before analyzing further details, it is worth noticing that, for $\Delta = 1$ and 0.5 , the scaling functions for each observable seem similar and apparently superpose to each other by considering an appropriate rescaling with nonuniversal metric factors, which indicates the existence of the universality class [79].

As shown in Fig. 9, the estimations of U_c obtained by collapsing $R_{m^2}(U, L)$ comparatively depend on L_{\min} ; however their dependency seems to be controllable, evenly approaching U_c^* that are determined by the crossing-point analysis in Fig. 3. The other estimations

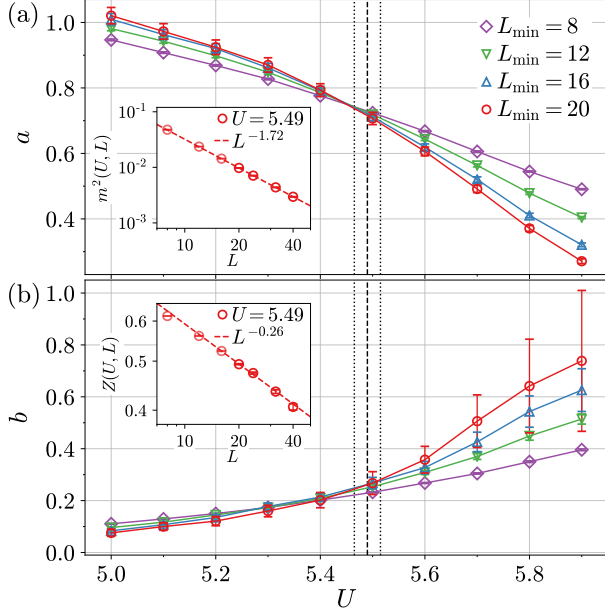


FIG. 6. U dependence of fitted exponents for $\Delta = 0.5$; (a) staggered magnetization $m^2(U, L)$ is fit to AL^{-1-a} and (b) quasiparticle weight $Z(U, L)$ is fit to BL^{-b} . Fitting range is between L_{\min} and L_{\max} ($= 40$). Vertical dashed and dotted lines indicate the critical point and the error bar, $U_c^* = 5.49(3)$, estimated from the crossing-point analysis of the correlation ratio in Fig. 3(b). Insets of panels (a) and (b) are log-log plots of $m^2(U_c^*, L)$ with $\eta_\phi = 0.72(4)$ and $Z(U_c^*, L)$ with $\eta_\psi = 0.26(3)$, respectively. Here, numbers in parentheses denote errors in the last digits.

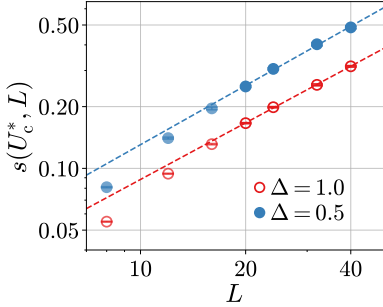


FIG. 7. Log-log fits of slopes of correlation ratio at the estimated critical point U_c^* . Open (solid) circles represent results for $\Delta = 1$ (0.5) with $U_c^* = 7.63$ (5.49). Dashed lines are fits to data for $L \geq 20$. Estimations of ν are $1.09(2)$ and $1.04(3)$ for $\Delta = 1$ and 0.5 , respectively. Here, numbers in parentheses denote errors in the last digits.

of U_c show the convergence to U_c^* already for $L_{\min} = 16$, except for the case of $m^2(U, L)$ for $\Delta = 0.5$.

Similar tendencies are observed in ν (see Fig. 10). For $L_{\min} \geq 16$, the values of ν fall almost between 1.0 and 1.1. Although it is not trivial to judge which estimation is most reliable, the candidate would be that obtained

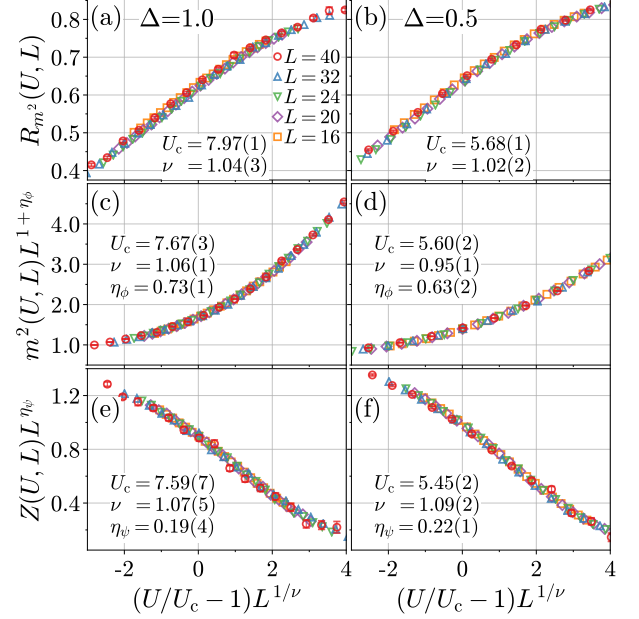


FIG. 8. Data-collapse fits of (a), (b) correlation ratio, (c), (d) staggered magnetization, and (e), (f) quasiparticle weight. For each observable, left and right figures show results of $\Delta = 1$ and 0.5 with the same scale. Estimated critical points and exponents are indicated in each figure. The number in parentheses indicates the statistical error, corresponding to the last digit of the value, which is estimated by the resampling technique [38].

from $R_{m^2}(U, L)$ for $\Delta = 1$, i.e., $\nu \simeq 1.05$, because the collapse fit of $R_{m^2}(U, L)$ includes the smaller number of the fitting parameters than the other observables, and the system with the isotropic Dirac cones for $\Delta = 1$ may have fewer correction effects.

The deviation of the exponents estimated from $m^2(U, L)$ for $\Delta = 0.5$ is further noticeable in η_ϕ , as shown in Fig. 11. To check which estimated values of η_ϕ are closer to the exact one, we also perform the data-collapse fits of $m^2(U, L)$ with U_c fixed at U_c^* , which is the most accurately obtained quantity in this study owing to the well-designed crossing-point analysis, whereas U_c estimated from the data-collapse fits of $m^2(U, L)$ sizably deviates from U_c^* for $\Delta = 0.5$ (see Fig. 9). As shown in Fig. 11, the exponent is converged to $\eta_\phi \simeq 0.75$ for both $\Delta = 1$ and 0.5 . This value is closer to the estimation of the isotropic case ($\Delta = 1$) with unfixed U_c and also to the results obtained from the scaling at the critical points shown in Figs. 5(a) and 6(a). Finally, Fig. 12 presents the results of η_ψ estimated from the data-collapse fits of $Z(U, L)$, in which the values of η_ψ for $\Delta = 1$ and 0.5 are confirmed to be coincident with each other.

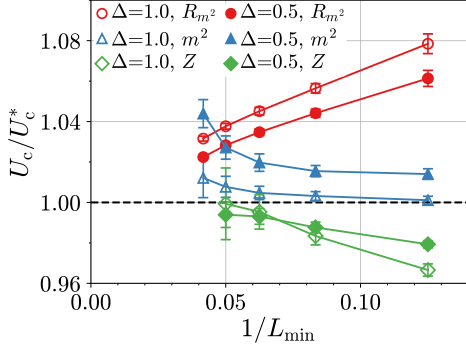


FIG. 9. $1/L_{\min}$ dependencies of the critical points U_c estimated from data-collapse fits of correlation ratio (circles), staggered magnetization (triangles), and quasiparticle weight (diamonds). For ease of comparison, values of U_c are normalized by $U_c^* = 7.63$ and 5.49 for $\Delta = 1$ (open symbols) and $\Delta = 0.5$ (solid symbols), respectively.

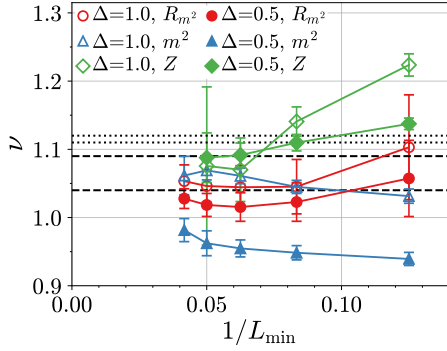


FIG. 10. $1/L_{\min}$ dependencies of the correlation-length exponent ν estimated from data-collapse fits of correlation ratio (circles), staggered magnetization (triangles), and quasiparticle weight (diamonds). Open (solid) symbols represent the results for $\Delta = 1$ (0.5). Dotted and dashed lines represent the estimations obtained from the crossing-point analysis in Figs. 4(a) and 4(b), and from the scaling at the critical point in Fig. 7, respectively.

IV. DISCUSSION AND CONCLUSIONS

Table I summarizes the critical exponents of our model estimated by the various methods. These exponents are also compared with those obtained by QMC calculations on other lattice models [37–39, 41] and by recent analytical studies on the GN model [44, 46–48], all for the $N = 8$ chiral-Heisenberg universality class.

Within the results of this work, the agreement of each exponent is mostly confirmed irrespectively of Δ . To be precise, the exception is found in the collapse fit of $m^2(U, L)$ for $\Delta = 0.5$. However, the difference in ν is marginally within two standard deviations, and the discrepancy in η_ϕ is resolved by fixing $U_c = U_c^*$. Therefore, our results represent accurate estimations of the critical exponents describing the chiral-Heisenberg universality

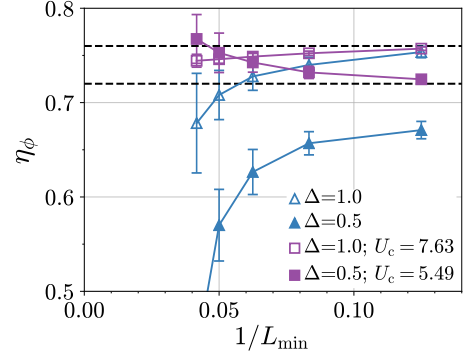


FIG. 11. $1/L_{\min}$ dependencies of the anomalous dimension of the order parameter η_ϕ estimated from data-collapse fits of staggered magnetization. Open (solid) triangles represent the results for $\Delta = 1$ (0.5). Results of the data-collapse fits with fixed $U_c = U_c^* = 7.63$ (5.49) for $\Delta = 1$ (0.5) are shown by open (solid) squares. Dashed lines represent the estimations obtained from the scaling at the critical points in Figs. 5(a) and 6(a).

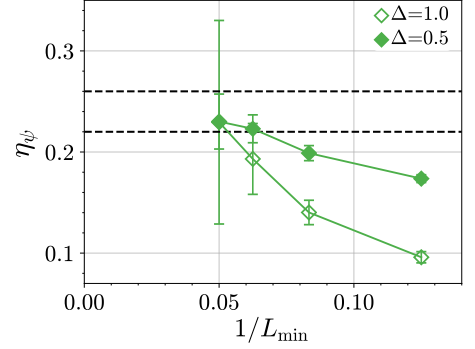


FIG. 12. $1/L_{\min}$ dependencies of the anomalous dimension of the fermionic field η_ψ estimated from data-collapse fits of quasiparticle weight. Open (solid) diamonds represent the results for $\Delta = 1$ (0.5). Dashed lines represent the estimations obtained from the scaling at the critical points in Figs. 5(b) and 6(b).

class. It is also stressed that the exponents are shared with the system with the anisotropic Dirac cones with $\Delta = 0.5$. In the previous studies, e.g., Ref. [38], it was shown that the isotropic Dirac Fermi velocity v_F^0 , which is different between the honeycomb lattice model and the π -flux model, does not affect the criticality. In addition, the present results indicate that the anisotropic velocity around the Dirac point is also irrelevant for the nature of the fixed point [57, 80–83].

Our results are comparable to the numerical results of the different lattice models [37–39, 41]. The estimations of ν and η_ψ are almost identical to the previous results that were reported by some of the present authors [38], while noticeable discrepancy is observed in η_ϕ . We here point out that the treatment of the correction term in the collapse fit of the staggered magnetization was presum-

TABLE I. Results of the critical exponents. Estimations obtained in this work are summarized in the upper group. For comparison, previous QMC results for other lattice models and recent analytical results for the Gross-Neveu model are also listed in the middle and lower groups, respectively.

Method	Δ	ν	η_ϕ	η_ψ
AFQMC (this work)				
$1/L \rightarrow 0$ of L and $2L$	1	1.12(8)	0.75(2)	0.23(4)
	0.5	1.11(17)	n.a.	0.29(4)
log-log fit at U_c^*	1	1.09(2)	0.76(3)	0.22(5)
	0.5	1.04(3)	0.72(4)	0.26(3)
data-collapse ^a of R_{m^2}	1	1.05(2)	—	—
	0.5	1.02(2)	—	—
data-collapse ^a of m^2	1	1.07(1)	0.71(3)	—
	1	—	0.75(1) ^b	—
	0.5	0.96(2)	0.57(4)	—
	0.5	—	0.75(2) ^b	—
data-collapse ^a of Z	1.0	1.08(12)	—	0.23(10)
	0.5	1.09(4)	—	0.23(3)
AFQMC ^c [38]		1.02(1)	0.49(4)	0.20(2)
			0.65(3) ^e	
AFQMC ^d [38]		1.02(1)	0.45(6)	0.23(2)
			0.64(6) ^e	
AFQMC ^c [37]		0.84(4)	0.70(15)	
AFQMC ^f [41]		0.88(7)	0.79(5)	
AFQMC ^g [43]		0.99(8)	0.55(2)	
HMC ^c [39]		1.162	0.872(44)	
4 - ϵ , 4th order [46]		1.2352	0.9563	0.1560
FRG [47]		1.26	1.032	0.071(2)
FRG [44]		1.314	1.012	0.083
Large N [48]		1.1823	1.1849	0.1051

^a $L_{\min} = 20$.

^b U_c is fixed at $U_c^* = 7.63$ (5.49) for $\Delta = 1$ (0.5).

^c SM-AF transition in the honeycomb lattice model.

^d SM-AF transition in the π -flux model.

^e Estimated by collapsing m^2 without the correction term.

^f SM to quantum spin-Hall transition on the honeycomb lattice.

^g d -wave SC to coexistence phase with gapped d -wave SC and AF order.

ably inaccurate, and instead the results of the collapse fits without the correction term for large L_{\min} , shown in Table I as well as in Table II of Ref. [38], are more reliable. More detailed reassessment on this point is left for future work. The estimated ν and η_ϕ of this work are also consistent with the recent AFQMC study on the Kane-Mele-like model showing a phase transition between SM and a quantum spin Hall insulator [41]. The agreement of the exponents reinforces the argument that this non-trivial phase transition belongs to the chiral-Heisenberg universality class.

The difference between the numerical and analytical results, although it is still noticeable, is decreased as compared with the previous situation reported in Ref. [38], mainly owing to technical advances such as higher-order calculations made possible recently [44, 46–

48]. Among them, the four-loop renormalization-group calculation [46] yields results closest to the present ones with a difference of the order of 25%, similar to the case of the chiral-XY universality class [33]. We expect that further efforts both in the numerical and analytical approaches will reconcile the remaining discrepancies.

Finally, we remark on a relation between U_c and the Dirac Fermi velocity in the noninteracting limit. In Ref. [37], it is suggested that the values of U_c are well scaled by the geometric mean \bar{v} of the velocities at the Dirac point. This is intuitively understood because, as shown in Eq. (8), \bar{v} appears in the density of states $D(E)$ near the Dirac point in the noninteracting limit as $D(E) = |E|/(\alpha\bar{v})^2$ with α being a constant $\alpha = \sqrt{\frac{V_{BZ}}{2\pi N_{\text{Dirac}}}}$. Indeed, our numerical simulations find that U_c scales with $\bar{v} = \sqrt{v_F v_\Delta}$, i.e.,

$$U_c/(\alpha\bar{v}) \simeq 2.15 \quad (\Delta = 1), \quad (27)$$

$$U_c/(\alpha\bar{v}) \simeq 2.19 \quad (\Delta = 0.5). \quad (28)$$

In addition, we find that these scaled values are close to those for the honeycomb lattice model and the π -flux model. Namely, using the values of U_c reported in Ref. [38], we find that

$$U_c/(\alpha v_F^0) \simeq 2.33 \quad (\text{honeycomb lattice model}), \quad (29)$$

$$U_c/(\alpha v_F^0) \simeq 2.21 \quad (\pi\text{-flux model}), \quad (30)$$

where $v_F^0 = 3t/2$ ($2t$) is the isotropic Dirac Fermi velocity in the noninteracting limit, and the value of α is calculated with $V_{BZ} = \frac{8\pi^2}{3\sqrt{3}} (2\pi^2)$ and $N_{\text{Dirac}} = 2$ for the honeycomb lattice model (π -flux model). We employ $\alpha\bar{v}$, instead of \bar{v} alone, as a measure of the energy scale, because the constant α compensates the difference among the models in the linear part of the density of states. These quantitative agreements strongly support the evidence that the effective theory for these lattice models is described by the same model in the continuous limit, i.e., the GN model.

To conclude, we have revisited the quantum criticality of the phase transitions for the chiral-Heisenberg universality class in terms of the Gross-Neveu model. The linear dispersion of the Dirac fermions is constructed by introducing a d -wave pairing field to the Hubbard model on the square lattice. Although the way of counting the number of fermion components is different, the resulting effective model is the same as that of the widely-studied Hubbard model on the honeycomb lattice. By exploiting large-scale quantum Monte Carlo simulations, we have calculated the correlation ratio of the spin structure factor, the staggered magnetization, and the quasi-particle weight. Based on these quantities, the antiferromagnetic phase transitions have been investigated by several methods such as the crossing-point analysis and the data-collapse fit. The conservative estimates for the critical exponents obtained in this work are $\nu = 1.05(5)$, $\eta_\phi = 0.75(4)$, and $\eta_\psi = 0.23(4)$. These results improve our previous estimates, especially for the exponent η_ϕ ,

which is now closer to the recent independent QMC calculation [41]. Indeed we have noticed that it is a cumbersome task to judge whether correction terms to the simple scaling ansatz should be included in a data-collapse fit of the Bayesian scaling analysis [78], and our previous estimates of η_ϕ [38] were eventually not accurate enough. We have also shown that the anisotropy of the Dirac cones does not affect the criticality, which suggests the emergent relativistic invariance at the quantum critical point.

ACKNOWLEDGMENTS

We acknowledge F. F. Assaad, T. Sato, F. Parisen Toldin, and Z. Wang for valuable comments. This

work has been supported by Grant-in-Aid for Scientific Research from MEXT Japan (under Grant Nos. 18K03475, 18H01183, and 19K23433) and by PRIN2017 MIUR prot.2017BZPKSZ. The numerical simulations have been performed on K computer provided by the RIKEN Center for Computational Science (R-CCS) through the HPCI System Research project (Project IDs: hp170162 and hp170328), and RIKEN supercomputer system (HOKUSAI GreatWave).

-
- [1] T.O. Wehling, A.M. Black-Schaffer, and A.V. Balatsky, “Dirac materials,” *Adv. Phys.* **63**, 1 (2014).
 - [2] O. Vafek and A. Vishwanath, “Dirac Fermions in Solids: From High- T_c Cuprates and Graphene to Topological Insulators and Weyl Semimetals,” *Annu. Rev. Condens. Matter Phys.* **5**, 83 (2014).
 - [3] S. Sorella and E. Tosatti, “Semi-Metal-Insulator Transition of the Hubbard Model in the Honeycomb Lattice,” *Europhys. Lett.* **19**, 699 (1992).
 - [4] Y. Otsuka and Y. Hatsugai, “Mott Transition in the Two-Dimensional Flux Phase,” *Phys. Rev. B* **65**, 073101 (2002).
 - [5] T. Paiva, R. T. Scalettar, W. Zheng, R. Singh, and J. Oitmaa, “Ground-state and finite-temperature signatures of quantum phase transitions in the half-filled Hubbard model on a honeycomb lattice,” *Phys. Rev. B* **72**, 085123 (2005).
 - [6] Z. Y. Meng, T. C. Lang, S. Wessel, F. F. Assaad, and A. Muramatsu, “Quantum Spin Liquid Emerging in Two-Dimensional Correlated Dirac Fermions,” *Nature* **464**, 847 (2010).
 - [7] S. Sorella, Y. Otsuka, and S. Yunoki, “Absence of a Spin Liquid Phase in the Hubbard Model on the Honeycomb Lattice,” *Sci. Rep.* **2**, 992 (2012).
 - [8] Y. Otsuka, S. Yunoki, and S. Sorella, “Quantum Monte Carlo study of the half-filled Hubbard model on the honeycomb lattice,” *J. Phys.: Conf. Ser.* **454**, 012045 (2013).
 - [9] Y. Otsuka, S. Yunoki, and S. Sorella, “Mott Transition in the 2D Hubbard Model with π -flux,” *JPS Conf. Proc.* **3**, 013021 (2014).
 - [10] D. Ixert, F. F. Assaad, and K. P. Schmidt, “Mott Physics in the Half-Filled Hubbard Model on a Family of Vortex-Full Square Lattices,” *Phys. Rev. B* **90**, 195133 (2014).
 - [11] Q. Chen, G. H. Booth, S. Sharma, G. Knizia, and G. K.-L. Chan, “Intermediate and Spin-Liquid Phase of the Half-Filled Honeycomb Hubbard Model,” *Phys. Rev. B* **89**, 165134 (2014).
 - [12] I. F. Herbut, “Interactions and Phase Transitions on Graphene’s Honeycomb Lattice,” *Phys. Rev. Lett.* **97**, 146401 (2006).
 - [13] I. F. Herbut, V. Juričić, and O. Vafek, “Relativistic Mott Criticality in Graphene,” *Phys. Rev. B* **80**, 075432 (2009).
 - [14] I. F. Herbut, V. Juričić, and B. Roy, “Theory of Interacting Electrons on the Honeycomb Lattice,” *Phys. Rev. B* **79**, 085116 (2009).
 - [15] S. Ryu, C. Mudry, C.-Y. Hou, and C. Chamon, “Masses in graphenelike two-dimensional electronic systems: Topological defects in order parameters and their fractional exchange statistics,” *Phys. Rev. B* **80**, 205319 (2009).
 - [16] D. Gross and A. Neveu, “Dynamical Symmetry Breaking in Asymptotically Free Field Theories,” *Phys. Rev. D* **10**, 3235 (1974).
 - [17] J. A. Gracey, “Three-loop calculations in the $O(N)$ Gross-Neveu model,” *Nucl. Phys. B* **341**, 403 (1990).
 - [18] A. N. Vasil’ev, S. É. Derkachev, N. A. Kivel’, and A. S. Stepanenko, “The $1/n$ Expansion in the Gross-Neveu Model: Conformal Bootstrap Calculation of the Index η in Order $1/n^3$,” *Theor. Math. Phys.* **94**, 127 (1993).
 - [19] B. Rosenstein and A. Kovner, “Critical Exponents of New Universality Classes,” *Phys. Lett. B* **314**, 381 (1993).
 - [20] L. Kärkkäinen, R. Lacaze, P. Lacock, and B. Petersson, “Critical behaviour of the three-dimensional Gross-Neveu and Higgs-Yukawa models,” *Nucl. Phys. B* **415**, 781 (1994).
 - [21] J. A. Gracey, “Computation of Critical Exponent η at $O(1/N^3)$ in the Four-Fermi Model in Arbitrary Dimensions,” *Int. J. Mod. Phys. A* **09**, 727 (1994).
 - [22] L. Rosa, P. Vitale, and C. Wetterich, “Critical Exponents of the Gross-Neveu Model from the Effective Average Action,” *Phys. Rev. Lett.* **86**, 958 (2001).
 - [23] F. Höfling, C. Nowak, and C. Wetterich, “Phase Transition and Critical Behavior of the $d = 3$ Gross-Neveu Model,” *Phys. Rev. B* **66**, 205111 (2002).
 - [24] L. Wang, P. Corboz, and M. Troyer, “Fermionic Quantum Critical Point of Spinless Fermions on a Honeycomb Lattice,” *New J. Phys.* **16**, 103008 (2014).
 - [25] Z.-X. Li, Y.-F. Jiang, and H. Yao, “Fermion-Sign-Free Majorana-Quantum-Monte-Carlo Studies of Quantum Critical Phenomena of Dirac Fermions in Two Dimensions,” *New J. Phys.* **17**, 085003 (2015).
 - [26] L. Wang, M. Iazzi, P. Corboz, and M. Troyer, “Efficient continuous-time quantum Monte Carlo method for the ground state of correlated fermions,” *Phys. Rev. B* **91**,

- 235151 (2015).
- [27] S. Hesselmann and S. Wessel, “Thermal Ising Transitions in the Vicinity of Two-Dimensional Quantum Critical Points,” *Phys. Rev. B* **93**, 155157 (2016).
 - [28] L. Wang, Y.-H. Liu, and M. Troyer, “Stochastic Series Expansion Simulation of the t - V Model,” *Phys. Rev. B* **93**, 155117 (2016).
 - [29] H. Xu, Z. Zhou, X. Wang, L. Wang, and Y. Wang, “Quantum Monte Carlo simulations of the attractive $SU(3)$ Hubbard model on a honeycomb lattice,” [arXiv:1912.11233](https://arxiv.org/abs/1912.11233).
 - [30] Y. Liu, W. Wang, K. Sun, and Z. Y. Meng, “Designer Monte Carlo simulation for the Gross-Neveu-Yukawa transition,” *Phys. Rev. B* **101**, 064308 (2020).
 - [31] E. Huffman and S. Chandrasekharan, “Fermion-bag inspired Hamiltonian lattice field theory for fermionic quantum criticality,” *Phys. Rev. D* **101**, 74501 (2020).
 - [32] Z.-X. Li, Y.-F. Jiang, S.-K. Jian, and H. Yao, “Fermion-induced quantum critical points,” *Nat. Commun.* **8**, 314 (2017).
 - [33] Y. Otsuka, K. Seki, S. Sorella, and S. Yunoki, “Quantum criticality in the metal-superconductor transition of interacting Dirac fermions on a triangular lattice,” *Phys. Rev. B* **98**, 035126 (2018).
 - [34] X. Y. Xu, K. T. Law, and P. A. Lee, “Kekulé valence bond order in an extended Hubbard model on the honeycomb lattice with possible applications to twisted bilayer graphene,” *Phys. Rev. B* **98**, 121406 (2018).
 - [35] B.-H. Li, Z.-X. Li, and H. Yao, “Fermion-induced quantum critical point in Dirac semimetals: A sign-problem-free quantum Monte Carlo study,” *Phys. Rev. B* **101**, 085105 (2020).
 - [36] F. F. Assaad and I. F. Herbut, “Pinning the Order: The Nature of Quantum Criticality in the Hubbard Model on Honeycomb Lattice,” *Phys. Rev. X* **3**, 031010 (2013).
 - [37] F. Parisen Toldin, M. Hohenadler, F. F. Assaad, and I. F. Herbut, “Fermionic Quantum Criticality in Honeycomb and π -flux Hubbard Models: Finite-size Scaling of Renormalization-Group-Invariant Observables from Quantum Monte Carlo,” *Phys. Rev. B* **91**, 165108 (2015).
 - [38] Y. Otsuka, S. Yunoki, and S. Sorella, “Universal Quantum Criticality in the Metal-Insulator Transition of Two-Dimensional Interacting Dirac Electrons,” *Phys. Rev. X* **6**, 011029 (2016).
 - [39] P. Buividovich, D. Smith, M. Ulybyshev, and L. von Smekal, “Hybrid Monte Carlo study of competing order in the extended fermionic Hubbard model on the hexagonal lattice,” *Phys. Rev. B* **98**, 235129 (2018).
 - [40] T. C. Lang and A. M. Läuchli, “Quantum Monte Carlo Simulation of the Chiral Heisenberg Gross-Neveu-Yukawa Phase Transition with a Single Dirac Cone,” *Phys. Rev. Lett.* **123**, 137602 (2019).
 - [41] Y. Liu, Z. Wang, T. Sato, M. Hohenadler, C. Wang, W. Guo, and F. F. Assaad, “Superconductivity from the condensation of topological defects in a quantum spin-Hall insulator,” *Nat. Commun.* **10**, 1 (2019).
 - [42] J. Ostmeyer, E. Berkowitz, S. Krieg, T. Luu, and C. Urbach, “The Semimetal-Mott Insulator Quantum Phase Transition of the Hubbard Model on the Honeycomb Lattice,” [arXiv:2005.11112v1](https://arxiv.org/abs/2005.11112v1).
 - [43] X. Y. Xu and T. Grover, “Competing nodal d-wave superconductivity and antiferromagnetism: a Quantum Monte Carlo study,” [arXiv:2009.06644](https://arxiv.org/abs/2009.06644).
 - [44] L. Janssen and I. F. Herbut, “Antiferromagnetic Critical Point on Graphene’s Honeycomb Lattice: A Functional Renormalization Group Approach,” *Phys. Rev. B* **89**, 205403 (2014).
 - [45] L. Classen, I. F. Herbut, and M. M. Scherer, “Fluctuation-induced continuous transition and quantum criticality in Dirac semimetals,” *Phys. Rev. B* **96**, 115132 (2017).
 - [46] N. Zerf, L. N. Mihaila, P. Marquard, I. F. Herbut, and M. M. Scherer, “Four-loop critical exponents for the Gross-Neveu-Yukawa models,” *Phys. Rev. D* **96**, 096010 (2017).
 - [47] B. Knorr, “Critical chiral Heisenberg model with the functional renormalization group,” *Phys. Rev. B* **97**, 075129 (2018).
 - [48] J. A. Gracey, “Large N critical exponents for the chiral Heisenberg Gross-Neveu universality class,” *Phys. Rev. D* **97**, 105009 (2018).
 - [49] B. Ihrig, L. N. Mihaila, and M. M. Scherer, “Critical behavior of Dirac fermions from perturbative renormalization,” *Phys. Rev. B* **98**, 125109 (2018).
 - [50] S. Pujari, T. C. Lang, G. Murthy, and R. K. Kaul, “Interaction-Induced Dirac Fermions from Quadratic Band Touching in Bilayer Graphene,” *Phys. Rev. Lett.* **117**, 086404 (2016).
 - [51] D. J. Scalapino, E. Loh, and J. E. Hirsch, “d-wave pairing near a spin-density-wave instability,” *Phys. Rev. B* **34**, 8190 (1986).
 - [52] P. A. Lee, “Localized states in a d-wave superconductor,” *Phys. Rev. Lett.* **71**, 1887 (1993).
 - [53] J. E. Drut and T. A. Lähde, “Is Graphene in Vacuum an Insulator?” *Phys. Rev. Lett.* **102**, 026802 (2009).
 - [54] In this paper, a d -wave BCS state with the Dirac quasi-particle dispersion is referred to simply as a semimetallic state.
 - [55] H. B. Nielsen and S. Chadha, “On how to count Goldstone bosons,” *Nucl. Phys. B* **105**, 445 (1976).
 - [56] H. Watanabe, “Counting Rules of Nambu-Goldstone Modes,” *Annu. Rev. Condens. Matter Phys.* **11**, 169 (2020).
 - [57] S. Sachdev, *Quantum Phase Transitions* (Cambridge University Press, Cambridge, 1999).
 - [58] M. Vojta, Y. Zhang, and S. Sachdev, “Quantum Phase Transitions in d-Wave Superconductors,” *Phys. Rev. Lett.* **85**, 4940 (2000).
 - [59] D. V. Khveshchenko and J. Paaske, “Incipient Nodal Pairing in Planar d-wave Superconductors,” *Phys. Rev. Lett.* **86**, 4672 (2001).
 - [60] Y. Otsuka, Y. Morita, and Y. Hatsugai, “Anisotropy on the Fermi surface of the two-dimensional Hubbard model,” *Phys. Rev. B* **66**, 073109 (2002).
 - [61] R. Blankenbecler, D. J. Scalapino, and R. L. Sugar, “Monte Carlo Calculations of Coupled Boson-Fermion Systems. I,” *Phys. Rev. D* **24**, 2278 (1981).
 - [62] J. E. Hirsch, “Two-dimensional Hubbard Model: Numerical Simulation Study,” *Phys. Rev. B* **31**, 4403 (1985).
 - [63] S. R. White, D. J. Scalapino, R. L. Sugar, E. Y. Loh, J. E. Gubernatis, and R. T. Scalettar, “Numerical Study of the Two-Dimensional Hubbard Model,” *Phys. Rev. B* **40**, 506 (1989).
 - [64] F. F. Assaad and H. G. Evertz, “World-line and Determinantal Quantum Monte Carlo Methods for Spins, Phonons and Electrons,” in *Computational Many-Particle Physics*, edited by Fehske

- H., Schneider R., Weiße. (Springer Berlin, 2008) pp. 277–356.
- [65] F. Becca and S. Sorella, [Quantum Monte Carlo approaches for correlated systems](#) (Cambridge University Press, Cambridge, 2017).
- [66] M. Suzuki, “Generalized Trotter’s Formula and Systematic Approximants of Exponential Operators and Inner Derivations with Applications to Many-Body Problems,” *Commun. Math. Phys.* **51**, 183 (1976).
- [67] H. F. Trotter, “On the Product of Semi-Groups of Operators,” *Proc. Amer. Math. Soc.* **10**, 545 (1959).
- [68] J. E. Hirsch, “Discrete Hubbard-Stratonovich Transformation for Fermion Lattice Models,” *Phys. Rev. B* **28**, R4059 (1983).
- [69] R. K. Kaul, “Spin Nematics, Valence-Bond Solids, and Spin Liquids in $SO(N)$ Quantum Spin Models on the Triangular Lattice,” *Phys. Rev. Lett.* **115**, 157202 (2015).
- [70] H. Shao, W. Guo, and A. W. Sandvik, “Quantum criticality with two length scales,” *Science* **352**, 213 (2016).
- [71] L. Wang, K. S. D. Beach, and A. W. Sandvik, “High-precision finite-size scaling analysis of the quantum-critical point of $S = 1/2$ Heisenberg antiferromagnetic bilayers,” *Phys. Rev. B* **73**, 014431 (2006).
- [72] S. Wenzel and W. Janke, “Comprehensive quantum Monte Carlo study of the quantum critical points in planar dimerized/quadrumerized Heisenberg models,” *Phys. Rev. B* **79**, 014410 (2009).
- [73] F.-J. Jiang and U. Gerber, “Subtlety of determining the critical exponent ν of the spin-1/2 Heisenberg model with a spatially staggered anisotropy on the honeycomb lattice,” *J. Stat. Mech.* **2009**, P09016 (2009).
- [74] N. Ma, P. Weinberg, H. Shao, W. Guo, D.-X. Yao, and A. W. Sandvik, “Anomalous Quantum-Critical Scaling Corrections in Two-Dimensional Antiferromagnets,” *Phys. Rev. Lett.* **121**, 117202 (2018).
- [75] X. Ran, N. Ma, and D.-X. Yao, “Criticality and scaling corrections for two-dimensional Heisenberg models in plaquette patterns with strong and weak couplings,” *Phys. Rev. B* **99**, 174434 (2019).
- [76] T. Sato, M. Hohenadler, T. Grover, J. McGreevy, and F. F. Assaad, “Topological terms on topological defects: a quantum Monte Carlo study,” (2020), [arXiv:2005.08996](#).
- [77] K. Seki, Y. Otsuka, S. Yunoki, and S. Sorella, “Fermi-liquid ground state of interacting Dirac fermions in two dimensions,” *Phys. Rev. B* **99**, 125145 (2019).
- [78] K. Harada, “Bayesian Inference in the Scaling Analysis of Critical Phenomena,” *Phys. Rev. E* **84**, 056704 (2011).
- [79] V. Privman and M. E. Fisher, “Universal Critical Amplitudes in Finite-Size Scaling,” *Phys. Rev. B* **30**, 322 (1984).
- [80] O. Vafek, Z. Tešanović, and M. Franz, “Relativity Restored: Dirac Anisotropy in QED₃,” *Phys. Rev. Lett.* **89**, 157003 (2002).
- [81] A. Sharma, V. N. Kotov, and A. H. C. Neto, “Interacting Anisotropic Dirac Fermions in Strained Graphene and Related Systems,” (2012), [arXiv:1206.5427](#).
- [82] J.-R. Wang and G.-Z. Liu, “Influence of Coulomb interaction on the anisotropic Dirac cone in graphene,” *Phys. Rev. B* **89**, 195404 (2014).
- [83] B. Roy, V. Juričić, and I. F. Herbut, “Emergent Lorentz symmetry near fermionic quantum critical points in two and three dimensions,” *J. High Energ. Phys.* **2016**, 18 (2016).